Technical Physics, 2022, Vol. 67, No. 11

01

Simulation of the features of the magnetic properties of axisummetric granules of hard type II superconductors

© *N.D. Kuzmichev, A.A. Shushpanov, M.A. Vasyutin*

Ogarev Mordovia State University, Saransk, Russia
e-mail: kuzmichevnd@yandex.ru

Received April 14, 2022
Revised July 6, 2022
Accepted July 11, 2022

Based on the equations of electrodynamics and the concept of a critical state for hard superconductors of the 2nd kind, numerical simulation of the magnetic properties of axisymmetric superconducting samples, in particular, granules, is performed for a number of models of the dependence of the critical current density on the magnetic field induction. The magnetic moment loops are calculated directly by integrating the integral equation for the current density over time. The phenomena of the peak effect and the asymmetry of the magnetization hysteresis loop are also considered using the indicated equation. Various versions of the functions used in the literature were used as peak functions. In addition to the hysteresis loop of the magnetic moment, the magnetic field induction at the center of axisymmetric samples, and the total penetration field, the profiles of the critical current density $J_c(B)$ and the equilibrium magnetic moment for spherical granules were obtained. The method used for calculating the magnetic moment of superconductors makes it possible to take into account the equilibrium and nonequilibrium regions of the magnetization of the samples independently

Keywords: magnetic moment, axisymmetric granules, type II superconductor, critical state, peak effect, equilibrium magnetic moment.

DOI: 10.21883/TP.2022.11.55168.98-22

Introduction

The expansion of the scope of superconducting materials has greatly increased scientific interest in the study of their properties, including magnetic ones. Measuring the parameters of known and new substances is one of the most important aspects of research. Basic characteristics of superconductors include, for example, critical current density and critical magnetic field values. To obtain them, non-contact indirect measurements are usually used. The obtained parameters, in turn, can be used to predict the behavior of the superconductor in other scenarios, which technically simplifies research.

Simple sample shapes are most often used for measurements: disks, cylinders, films, parallelepipeds, ellipsoids, etc.Most of modern synthesized crystalline superconducting materials have a granular structure and in the first approximation can be represented as a set of microscopic spheres, ellipsoids or cylinders. For such samples, the problem acquires axial symmetry, which facilitates the modeling task. In this case, the current trajectories become coaxial circles, and the problem is reduced to a two-dimensional distribution of the basic electric and magnetic quantities: current density J, vector potential A, electric E and magnetic H fields. One of the first models describing the magnetization of rigid superconductors of type II kind was proposed by C. Bin [1]. It assumed that in fields exceeding the first critical field H_{c1}, the current density takes a constant value equal to the critical density J_c in areas of magnetic field penetration (i.e., where Abrikosov filaments fixed on heterogeneities were formed). In reality, the superconductor behavior is influenced by many more factors, and the distribution of current within the sample becomes very complicated. It largely depends on the movement of magnetic field carriers (Abrikosov filaments (vortices)). The strength of their interaction with the superconductor material (pinning, displacement, formation of structures, etc.) will largely determine the behavior of the sample in the magnetic field. As a result, all this causes more complex effects: the field dependence of the critical current density, the peak effect, equilibrium magnetization zones, temperature dependences of parameters, etc.

The aim of this work is to numerically simulate some features of magnetic properties of homogeneous rigid superconductors of the second kind (RSSK) with axial symmetry (ellipsoids of rotation, cylinders, etc.), in particular, pellets in homogeneous magnetic fields parallel to the symmetry axis of samples. The simulations are performed using different field dependencies of the critical current density. The phenomena of the peak effect and equilibrium magnetization are considered. The numerical calculations performed in this work are based on the works [2,3], in which the magnetic properties of plates, disks, and short cylinders were determined within the Bin and Kim models using the integral equation of the second kind. For ellipsoids of rotation and cylinders, similar calculations are made in works [4,5]. It should be noted that there are other approaches currently used to describe the magnetic properties of finite-size superconductors, based on the stationary [6,7] and non-stationary [8] Ginzburg-Landau

equations. These descriptions lead to a deeper understanding of the magnetization mechanism of superconductors, but these equations are nonlinear differential equations and require additional setting of boundary and initial conditions, which greatly complicates the problem.

1. Electric current equation

As noted in the introduction, the numerical simulation of the critical state of the RSSK performed in this paper is based on the methodology of works [2,3]. The calculation methodology applied in the above papers can be extended to any axisymmetric shapes and other models when considering more complex effects.

We will work in the cylindrical coordinate system r, φ, z. Let's orient the z axis along the symmetry axis of the sample and set its boundaries: $-b \le z \le b,\ r(z) \le a(z)$, where b — half-height of the sample, and $a(z)$ — radius of the sample in the section with coordinate z. If it has a horizontal symmetry plane, the position$(0, 0)$ is chosen at the center of the sample. In the general case (e.g., to define a tapered shape), you can move the origin to the bottom-most point.

Let's consider a magnetic isotropic RSSK with linear isotropic dependence of magnetic field induction on its intensity $\mathbf{B} = \mu_0\mu\mathbf{H}$ ($\mu = 1$, μ_0 — magnetic constant). To describe the electrical properties, it is necessary to introduce an analogue of the volt-ampere characteristic (VAM) — the dependence of the electric field strength vector on the current density $\mathbf{E}(\mathbf{J})$, which can be represented as: $\mathbf{E} = E(J)\mathbf{J}/J$. For the correctness of the calculations, following the works [2,3], we will use as $E(J)$ a fast-growing smooth function, a good approximation of which is a power function with a large exponent rr:

$$E(J) = E_c(J/J_c)^n. \tag{1}$$

Here, J_c — the critical current density, and E_c —the corresponding electric field strength.

In addition, Maxwell's equations for the magnetic field and the London calibration for the vector potential will be used. The initial system of equations has the form:

$$\begin{cases} \mathbf{E} = \frac{E(J)\mathbf{J}}{J}, \\ \mathbf{B} = \mu_0\mathbf{H}, \\ \mathbf{J} = \nabla \times \mathbf{H}, \\ \dot{\mathbf{B}} = -\nabla \times \mathbf{E}, \\ \nabla \times \mathbf{A} = \mathbf{B}, \\ \nabla \cdot \mathbf{A} = 0. \end{cases} \tag{2}$$

Transforming this system, we obtain the Poisson equation for the vector potential

$$\mu_0\mathbf{J} = -\nabla^2(\mathbf{A} - \mathbf{A}_a).$$

Here, $\mathbf{A}_a$ — the vector potential of the external magnetic field. In axial symmetry, when the induction of the external magnetic field $\mathbf{B}_a$ is directed along the axis, the equation will be

$$\mu_0 J = -\nabla^2\left(A + \frac{r}{2}B_a\right). \tag{3}$$

Here, the vectors $\mathbf{A}, \mathbf{A}_a$ and $\mathbf{J}$ have the same azimuthal component and are respectively equal: $A, A_a = -(r/2)B_a$ and J.

The solution of equation (3) can be obtained using the Green's function in the cylindrical coordinate system [3,5,9]:

$$A(\mathbf{r}) = -\mu_0 \int_0^a dr' \int_0^b dz' G_{cyl}(\mathbf{r}, \mathbf{r}')J(\mathbf{r}') - \frac{r}{2}B_a, \tag{4}$$

where $\mathbf{r} = (r, z)$, $\mathbf{r}' = (r', z')$. The integral kernel (Green's function) is expressed through elliptic functions:

$$G_{cyl}(\mathbf{r}, \mathbf{r}') = f(r, r', z - z') + f(r, r', z + z').$$

where

$$f(r, r', z) = \int_0^\pi \frac{d\varphi}{2\pi} \frac{-r'\cos\varphi}{(z^2 + r^2 + r'^2 - 2rr'\cos\varphi)^{1/2}}. \tag{5}$$

For shapes that do not have a horizontal symmetry plane, a simplified kernel form should be used: $G_{cyl}(\mathbf{r}, \mathbf{r}') = f(r, r', z - z')$.

When the external magnetic field changes $\mathbf{B}_a = \mathbf{B}_a(t)$, the current density inside the superconductor $J = J(\mathbf{r}, t)$ also changes. Take the time derivative of equation (4) (dot above the letter denoting the function). Then, using the system of equations (2), we obtain:

$$E(J(\mathbf{r}, t)) = \mu_0 \int_0^a dr' \int_0^b dz' G_{cyl}(\mathbf{r}, \mathbf{r}')\dot{J}(\mathbf{r}', t) + \frac{r}{2}\dot{B}_a(t).$$

Express the derivative $\dot{J}(\mathbf{r}, t)$ under the integral sign, using the inverse kernel $G^{-1}_{cyl}(\mathbf{r}, \mathbf{r}')$ and substitute the explicit form of the current-voltag curve (1) into the resulting first order nonlinear time differential equation for current density (electric current equation) [3]

$$\dot{J}(\mathbf{r}, t) = \mu_0^{-1} \int_0^a dr' \int_0^b dz' G^{-1}_{cyl}(\mathbf{r}, \mathbf{r}') \times \left[E_c\left(\frac{J(r, r')}{J_c}\right)^n - \frac{r'}{2}\dot{B}_a(t)\right]. \tag{6}$$

This equation allows us to trace the dynamics of changes in the local current densities inside the superconductor. We will use numerical solution methods to obtain the complete current distribution inside the superconductor.

2. Numerical method of calculation

Let's introduce a grid, along which we will divide the homogeneous sample into elementary sections. Let's make it non-uniform, with the cells compacted closer to the edges, which will allow a better description of the edge effects. The discrete variables of equation (6) $\mathbf{r}_k$ and $\mathbf{r}'_m$ have coordinates (r_i, z_j),in the cylindrical system, where $i = 1, \ldots, N_r$; $j = 1, \ldots, N_z$; $k, m = 1, \ldots, N_z N_r$. Let us introduce new variables u and v, which were used earlier in [5], different from the variables in [2,3]:

$$r_i = r_i(u_i) = \sin(u_i) \cdot a(z_i), \quad z_j = z(v_j) = \sin(v_j) \cdot b,$$

$$u_i = \frac{\frac{\pi}{2}(i - \frac{1}{2})}{N_r}, \quad v_j = \frac{\frac{\pi}{2}(j - \frac{1}{2})}{N_z}.$$

We replace the differentials dr' and dz' in (6) by discrete weight functions according to the differentiation rules:

$$dr'_i = (r'_i)' di \to \frac{\pi}{2} \cos u_i \frac{a(z_i)}{N_r} = \omega_r,$$

$$dy'_j = (y'_j)' dj \to \frac{\pi}{2} \cos v_j \frac{b}{N_z} = \omega_z,$$

Then, for example, the „weight" of a single cell with coordinate $\mathbf{r}_m$ would be defined as $\omega_m = \omega_r \omega_z$. The kernel of the integral $G_{cyl}(\mathbf{r}, \mathbf{r}')$ reduces to the matrix $G_{cyl}(\mathbf{r}_k, \mathbf{r}'_m) = G_{km}$. The electric current equation (6) reduces to the sum (discrete analog)

$$\dot{J}(\mathbf{r}_k, t) = j_k(t) = \sum_m (G_{km}\omega_m)^{-1} \left[E_c \left(\frac{J_m(t)}{J_{cm}} \right)^n - \frac{r_k}{2} \dot{B}_a(t) \right]. \tag{7}$$

The function $f(r, r', \eta)$ was calculated using the linear grid u_i:

$$u_i = \frac{i - 1/2}{M}, \; i = 1, 2, \ldots, M; \; M = 30;$$

$$\phi(u_i) = \pi u_i - \sin(\pi u_i).$$

The function (5) in the new variables has the form

$$f = \int_0^1 g[\phi(u)]\phi'(u) du \approx \frac{1}{M} \sum_{i=1}^{M} g[\phi(u_1)]\phi'(u_i),$$

where

$$g[\phi(u_i)] = \frac{1}{2\pi} \frac{r' \cos\phi(u_i)}{(\eta^2 + r^2 + r'^2 - 2rr' \cos\phi(u_i))^{1/2}},$$

$$\phi'(u_i) = \pi - \pi \cos(\pi u_i), \quad du_i = \frac{1}{M} di \to \frac{1}{M}.$$

The magnetic moment of the sample at the moment will be determined by the expression

$$m(t) = 2\pi \int_0^a dr r^2 \int_0^b dz J(r, z, t) \to m(t)$$

$$= 2\pi \sum_k r_k^2 \omega_k J_k(t). \tag{8}$$

The calculations were performed using a package of application programs. For this purpose, the electric current equation (6) was reduced to the matrix form (7):

$$\dot{\mathbf{J}}(t) = (\mathbf{GW})^{-1} \left[E_c(\mathbf{J}(t) \, \text{Ø} \, \mathbf{J}_c(t))^{\circ n} - \frac{\mathbf{R}}{2} B_a(t) \right],$$

where $\dot{\mathbf{J}} - (\dot{J}_{k1})$ — matrix-column of time derivatives of current density for each grid element, $\mathbf{G} = (G_{km})$ — square matrix of the equation kernel, $\mathbf{W} = diag(\omega_k)$ —diagonal matrix of grid cell weights, $\mathbf{J} = (J_{k1})$ and $\mathbf{J}_c = (\mathbf{J}_{ck1})$ — column matrices of the current and critical current densities in the grid cells, $\mathbf{R} = (r_{k1})$ —column matrix of r-cell coordinates, $\circ n$ — element-by-element matrix exponentiation, Ø — element-by-element division of matrices. To obtain the complete distribution of current densities $\mathbf{J}$, this equation is solved for each time moment with step τ and the initial condition $\mathbf{J}(0) = 0$: $\mathbf{J}(t + \tau) = \mathbf{J}(t) + \dot{\mathbf{J}}(t)\tau$.

We obtain the local magnetic field induction by numerically determining the rotor from the vector-potential (4):

$$\mathbf{B}(\mathbf{r}) = \nabla \times \mathbf{A}$$

$$= -\nabla \times \left[\mu_0 \int_0^a dr' \int_0^b dz' G_{cyl}(\mathbf{r}, \mathbf{r}') J(\mathbf{r}') + \frac{r}{2} B_a \right]. \tag{9}$$

Due to the axial symmetry, the vector $\mathbf{A}$ will have only an azimuthal projection, which simplifies the calculation of the vector $\mathbf{B}$, which has r and z components:

$$B_{ij} = \sqrt{(B_r^2)_{ij} + (B_z^2)_{ij}},$$

where

$$B_{r_{ij}} = -\frac{A_{i,j+1} - A_{i,j}}{z_{j+1} - z_j}, \; B_{z_{ij}} = \frac{A_{i+1,j} r_{i+1} - A_{i,j} r_i}{r_i(r_{i+1} - r_i)},$$

$i = 1, 2, \ldots, N_r - 1$, $j = 1, 2, \ldots, N_z - 1$.

Matrix A_{ij} of size $N_r \times N_y$ is obtained from the column matrix

$$\mathbf{A} = -\mu_0 \mathbf{GWJ} - \frac{\mathbf{R}}{2} B_a.$$

3. Magnetic moment hysteresis loops for a series of dependences of the critical current density on the magnetic field induction

Based on the above technique, let us consider the hysteresis curves of the magnetic moment of spherically symmetric homogeneous samples, in particular pellets, using a number of different field dependences of the critical current density used in the literature. The effect of the magnetic field on the critical current density is due to the fact that the resulting shielding induction current interacts with Abrikosov vortices in the area of their penetration. The vortices are fixed on heterogeneities of the material or come

into motion with a sufficient Lorentz force from the resulting shielding current. Since the force depends on the local magnetic field strength and the current flowing at that point, the critical current density is limited by the minimum force F_p (pinning force) sufficient to start vortex motion. In other words, $J = f(F_p, H)$. Different samples show differences in the pinning force dependences, as well as in the values of the second critical field H_{c2}. Based on this, the choice of the dependence $J(B)$ is made through comparison with experimental magnetization loops in similar samples. Their consistency serves as the main criterion for selecting the dependencies $J(B)$.

The following models were used in the present work. One of the first dependencies describing the decay of the critical current density as the magnetic field grows was proposed by Kim [10]:

$$J_c(B) = \frac{J_{c0}}{(1 + \frac{|B|}{B_0})}. \quad (10)$$

The model describes well the behavior of the superconductor in small fields $H \ll H_{c2}$. For fields close to H_{c2}, the dependence $J_c(B)$ better describes the model [11,12] with the dependence of the critical current $J_c(B) = J_{co}e^{-|B|/B_0}$.

The following was also used:
combined two-parameter form

$$J_c(B) = J_{c0}\Big(1 + \frac{|B|}{B_0}\Big)^{-\alpha} \quad (11)$$

and the three-parametric proposed in [13,14] et al.

$$J_c(B) = J_{c0}\frac{1 - (\frac{|B|}{B_{c2}})^{\alpha}}{1 + (\frac{|B|}{B_0})^{\alpha}}. \quad (12)$$

The latter dependence accounts for the behavior of the superconductor at different scales by accounting for the second critical field $B_{c2} = \mu_0 H_{c2}$.

For the calculation, we chose samples in the form of balls, the shape of the lateral boundary is described by the equation: $a(z) = a_0(1 - z^2)^{1/2}$, $a_0 = b = 1$. The density of the grid on which the calculation was made is 15 cells per unit length. All constants in the matrix equations for convenience were taken as one: $E_c = J_{c0} = \dot{B}_a = \mu_0 = \mu = 1$. „Speed of calculation“ (time step) — $\tau = 8 \cdot 10^{-6}$ s.The degree of the current-voltage curve is chosen by a large odd number n, as in the work [3]. Reducing n a few times, for example, from $n = 51$ to 11, leads to a small increase in magnetic moment ($\sim 9\%$) without qualitatively changing the hysteresis pattern of the loop. In the calculations, all magnetic field strength values were normalized to $J_{c0}a_0$ and magnetic moment values to $J_{c0}a_0^4$. The index of degree α was taken to be 0.5, and $B_{c2} = 20\,\mu_0 J_{c0} a_0$.

A complete magnetization cycle in a uniformly varying magnetic field was calculated for each model. The graphs below (Fig. 1) show the calculated magnetic moment loops $m(H_a)$ of the samples with variation of the main parameters based on formulas (10)−(12). Also presented here are the hysteresis loops $B(H_a)$, where B — magnetic field induction in the center of the sample, H_a — external field strength and $H_{a,\max}$ — maximum field strength of the magnetization cycle.

From the magnetic moment loop graphs in Fig. 1, *a, c, e, g*, we can see that the magnetic moment corresponding to the dependence (11) decreases more slowly with increasing H_a due to the slow decrease of J_c(B). The magnetic moment corresponding to formula (12) has a sharper peak near zero of the external field. In general, the curves $m(H_a)$ have a similar appearance. Fig. 1, *b, d, f, h* shows the hysteresis curves of the field induction $B(H_a)$ at the center of the sample, which show that the dependence J_c(B) (11) gives a wider loop, as in the case $m(H_a)$. In addition, the curve $B(H_a)$ in Fig. 1, *h* at $H_{a,\max} = 0.5J_{c0}a_0$ is missing, since $H_{a,\max} < H_p$ — full penetration fields.

In addition to obtaining the magnetic moment loops, the calculation was made of the total penetration field H_p depending on the values of the main parameter $B_0 = \mu_0 H_0$ of ellipsoidal samples with different ratios of half axes $a_0/b = 0.5, 1, 2$, for different models of the field dependence of the critical current density $J_c(B)$ ((10)−(12)) with the same parameters B_{c2} and α. The results are shown in Fig. 2.

The field of total penetration H_p into the sample (H_p — is the magnetic field strength when the vortex density (magnetic flux density B) and shielding supercurrent will be different from zero in the central area of the sample) was calculated for a uniformly growing external magnetic field. Then, at each counting step, the condition $B > 0.05\,\mu_0 J_{c0} a_0$ was checked. When it was performed, the external magnetic field was considered to penetrate into the sample and its value H_p was fixed. If you reduce the size of the cells, this condition can be reduced. When the density of cells per unit length was increased from 15 to 30, the field H_p changed insignificantly. The figure shows that the curves $H_p(H_0)$ show a monotonic increase with the exit to saturation. The curves also show, that elongated samples require a smaller field H_p, and flattened ones — a larger field. From a comparison of the graphs of $H_p(H_0)$ with each other, it follows that the dependence $J_c(B)$ (11) corresponds to a large field H_p.

4. Peak effect

The functions approximating the dependence of the critical current density on the local magnetic field induction suggest that it decreases monotonically as the field increases, which agrees with most experiments. However, some superconductors exhibit an increase in the macroscopic current density in some area instead of its monotonic decrease. This effect is reflected as a secondary maximum on the magnetization loops. There may be many reasons for this effect, such as reducing the stiffness of the vortex lattice, the effect of intergranular boundaries,

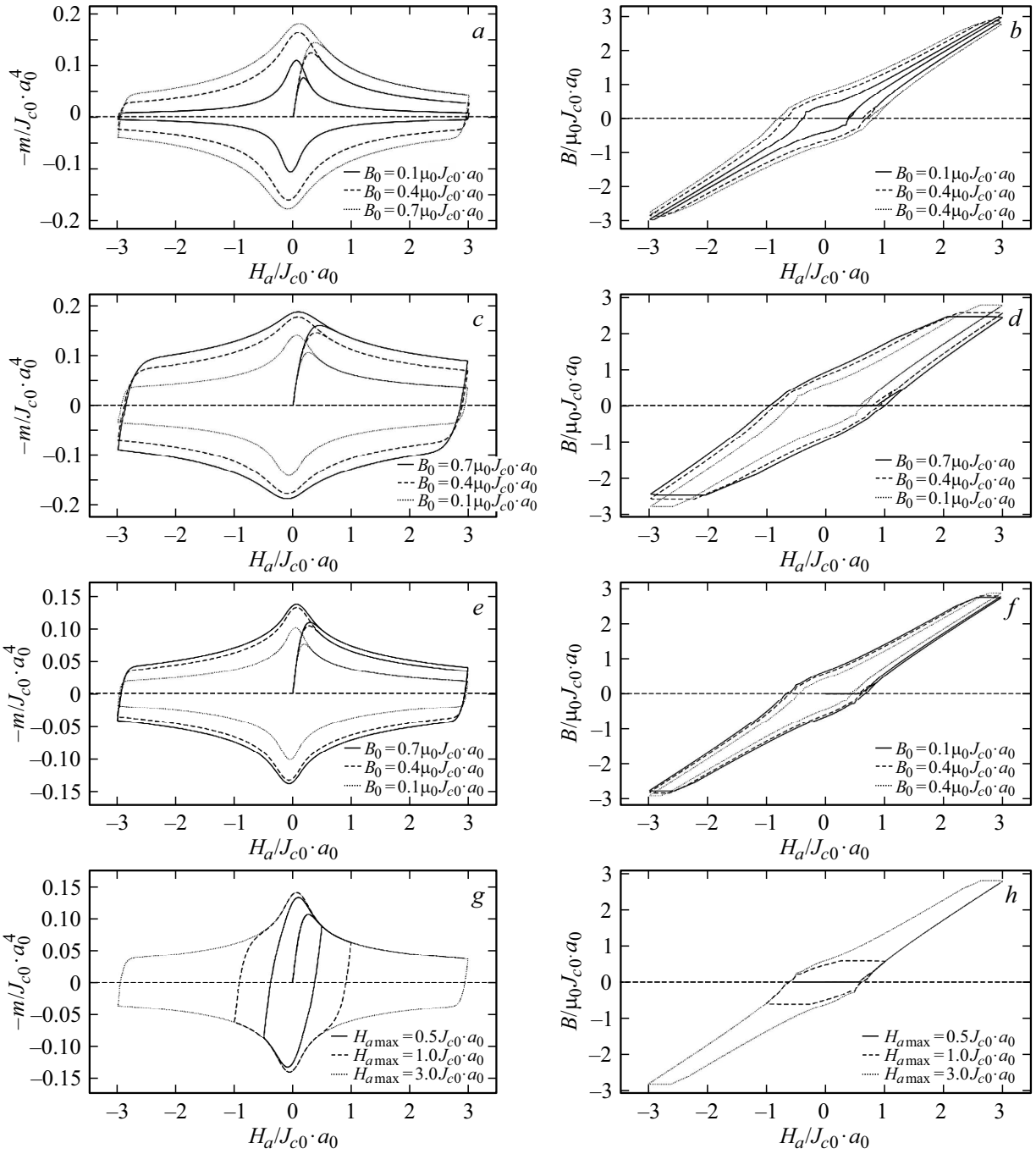

Figure 1. Magnetic moment (a, c, e, g) loops, and the dependence of the magnetic field induction at the center (b, d, f, h) of the superconducting ball for different values of parameter B_0 and dependences $J_c(B)$ (from the top down: (10) — a, b, (11) — c, d, (12) — e, f). Magnetic moment loops for $J_c(B)$ ((11) — g, h) at different values of the maximum field $H_{a,\max}$ of the magnetization cycle. The values of B_0 in the figures are shown in units of $\mu_0 J_{c0} a_0$.

the phase transition of the vortex lattice, phase separation, etc. In order to model this effect, it has been proposed in [15–18], etc., to modify the function $J_c(B)$ as follows. An additional term determining the shape of the secondary maximum is added to the $J_c(B)$ dependence models:

$$J_c(B) = J_{c0}(B)(1 + f_{peak}(B)). \tag{13}$$

The following functions [15–18] were used as the peak function f_{peak} in this paper:

$$f_{peak}(B) = A/\left(1 + \left(\frac{|B| - B_p}{B_w}\right)^2\right), \tag{14}$$

$$f_{peak}(B) = \frac{A|B|}{B_p}\exp\left(-\frac{(|B| - B_p)^2}{2B_w^2}\right), \tag{15}$$

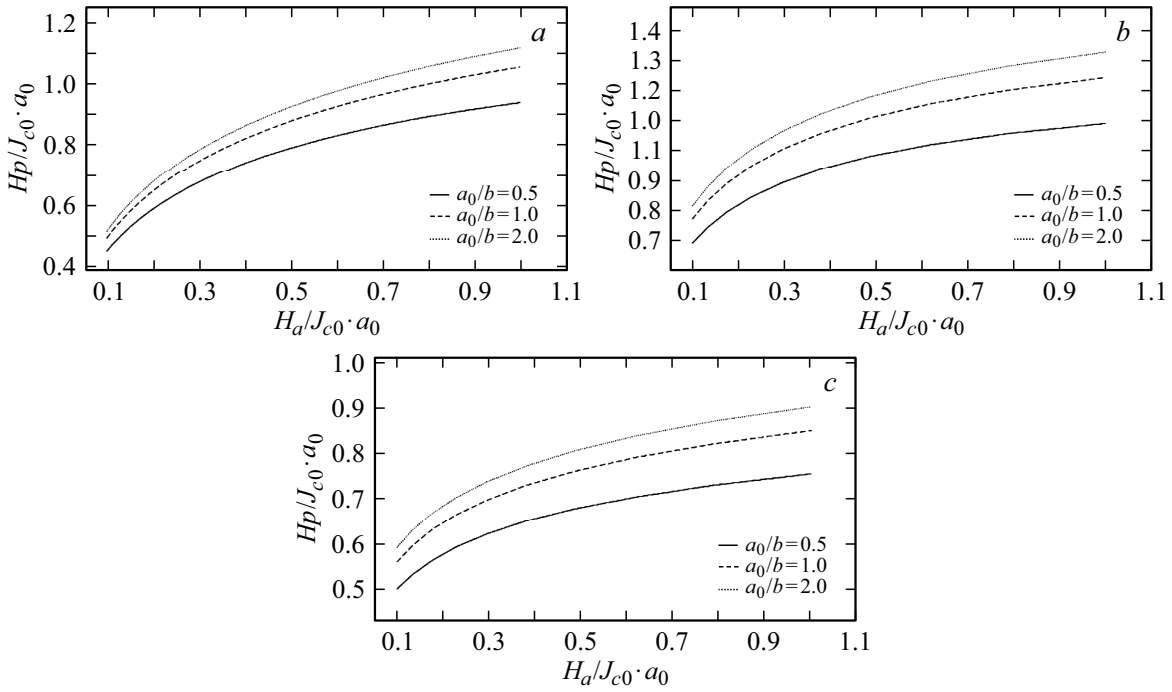

Figure 2. Dependence of the total penetration field H_p on the parameter $H_0 = B_0/\mu_0$ for ellipsoids with different semi-axis ratios $a_0/b = 0.5, 1, 2$ using different models $J_c(B)$: a — (10), b — (11), c — (12).

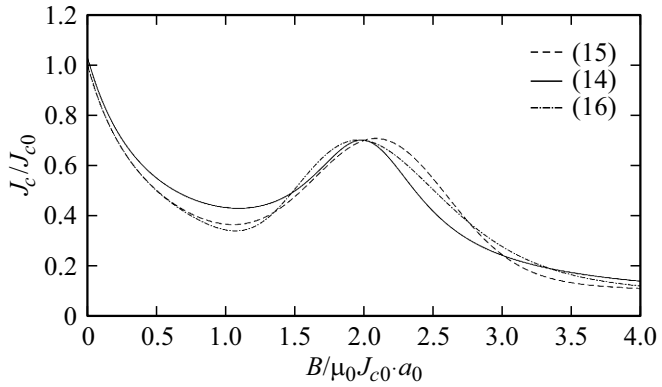

Figure 3. View of the critical current density function using the peak functions (14)–(16) with parameters $A = 0.5$, $B_p = 2\,\mu_0 J_{c0} a_0$, $B_w = 0.5\,\mu_0 J_{c0} a_0$.

$$f_{peak}(B) = A\exp\left(-\frac{(\frac{\ln|B|}{B_p})^2}{2(\frac{B_w}{B_p})^2}\right). \qquad (16)$$

Here, B_p — the field corresponding to the peak maximum; B_w — the field characterizing the peak width; A — the peak amplitude.

Fig. 3 shows a comparison of peak functions with the same parameters. As you can see, all of the features are quite similar in shape with equal width, height and position parameters. The advantage of using functions (15) and (16) is their value at zero field: $f_{peak}(0) = 0$, which does not change the maximum critical current density. In Section 4, the results of modeling the magnetization hysteresis loop of a spherical sample of radius a_0 in the Kim field dependence model using different peak-functions (14)–(16) and variation of their parameters will be presented.

From the analysis of the results shown in Fig. 4, it follows that all three functions (14)–(16) have no significant effect on the differences in the magnetic moment hysteresis loops. In addition, the influence of the parameters determining the width and position of the peak in the dependences $J_c(B)$ and $m(H_a)$ is the same.

The current density profiles $J_c(B(r, z))$ for a ball pellet of radius a_0 in the Kim model (1) with peak function (16) for three external field values $H_a = J_{c0}a_0$ were also calculated, $2J_{c0}a_0$ and $3J_{c0}a_0$, $2J_{c0}a_0$ and $3J_{c0}a_0$, which are obtained for the increasing field. The results are shown in Fig. 5 and 6. The figures show that there is a significant difference only when $H_a = J_{c0}a_0$ at the poles of the ball.

5. Equilibrium magnetization accounting

In fields $H > H_{c1}$ near the superconductor surface, Abrikosov vortices are formed, which are uniformly distributed in the superconductor in the absence of the pinning phenomenon, and the magnetic moment of the sample is also independent of the prehistory. In the case of pinning, the vortices formed near the surface are fixed on inhomogeneities. In the vortex-filled area, according to the critical state model [1,10], a screening current equal to the depinning current $I_c(B)$ flows. In this case, the magnetic moment will depend on the prehistory of the supercon-

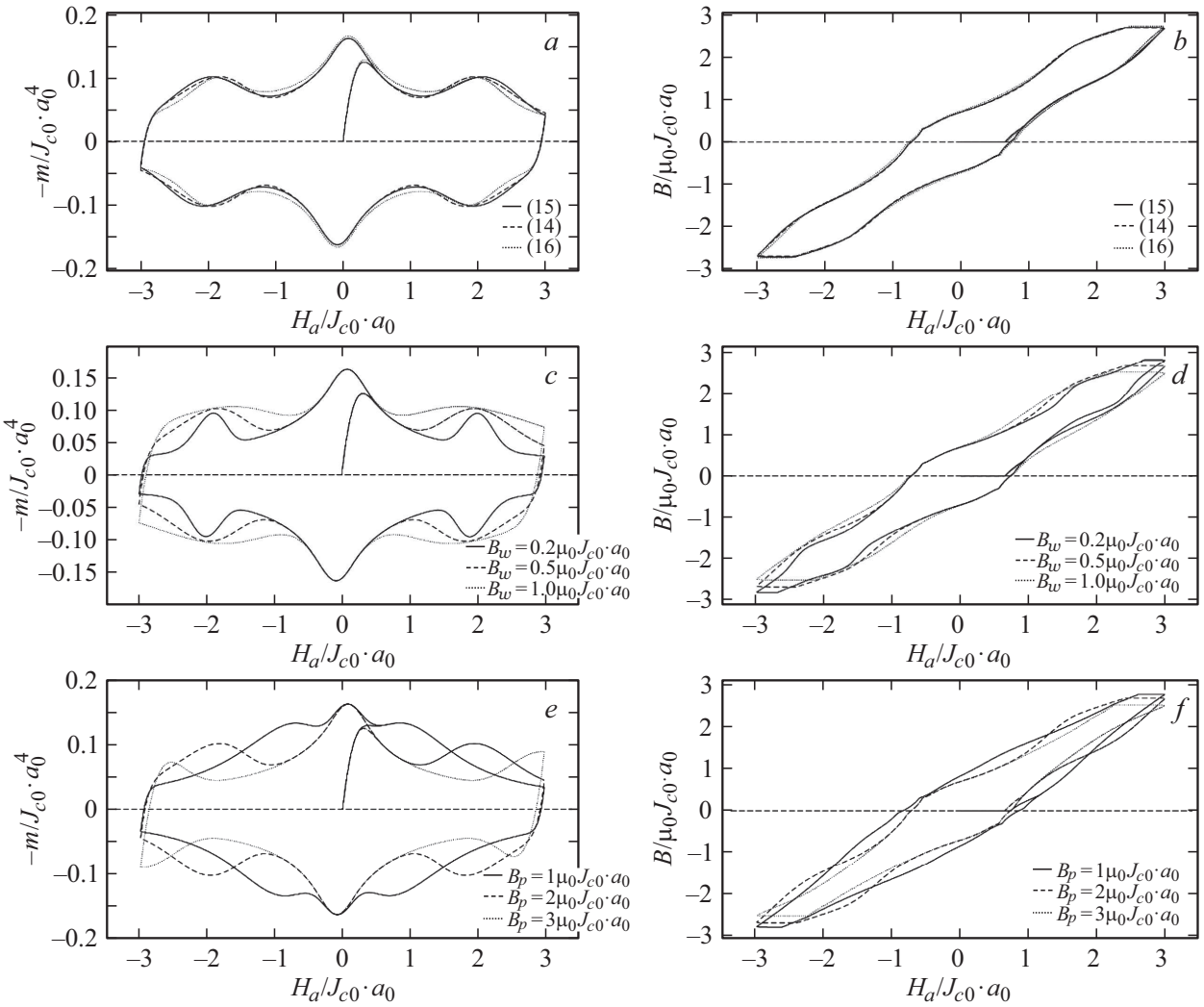

Figure 4. Magnetic moment loops (a, c, e) and magnetic field values in the center of the samples (b, d, f). a, b — data are given for different peak functions (14)–(16) with the same parameters: $A = 0.3$, $B_p = 2\mu_0 J_{c0} a_0$, $B_w = 0.5\mu_0 J_{c0} a_0$; c, d — for different widths; e, f — for different positions of the secondary peak. The values of the changeable parameters are shown in the figures. In other cases, the values $A = 0.3$, $B_p = 2\mu_0 J_{c0} a_0$, $B_w = 0.5\mu_0 J_{c0} a_0$ were used, and function (16) was used as peak function on the second and third rows.

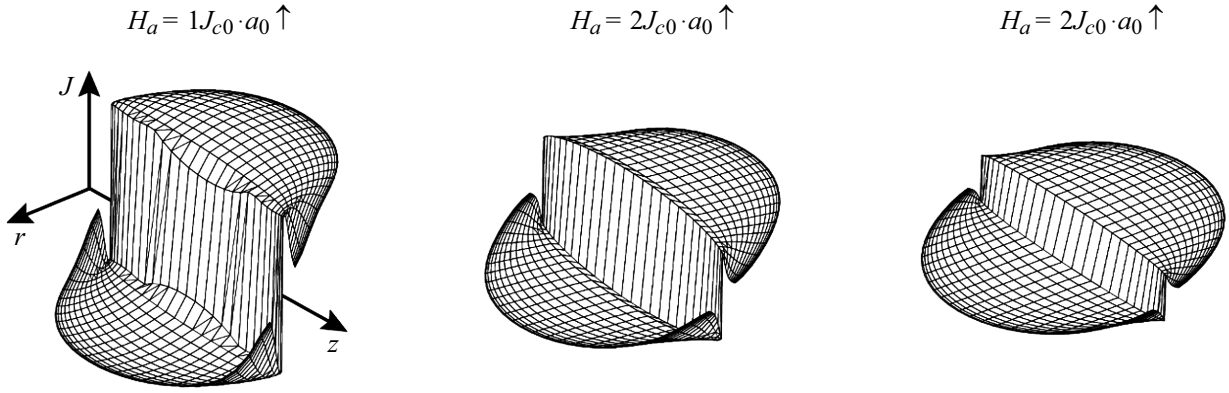

Figure 5. Current density profiles $J_c(B(r, z))$ for a ball of radius a in the Kim model (10) with peak effect (16) for three external field values $H_a = 1J_{c0}a_0$, $2J_{c0}a_0$ and $3J_{c0}a_0$. The position of the maximum is $B_p = 2\mu_0 J_{c0} a_0$.

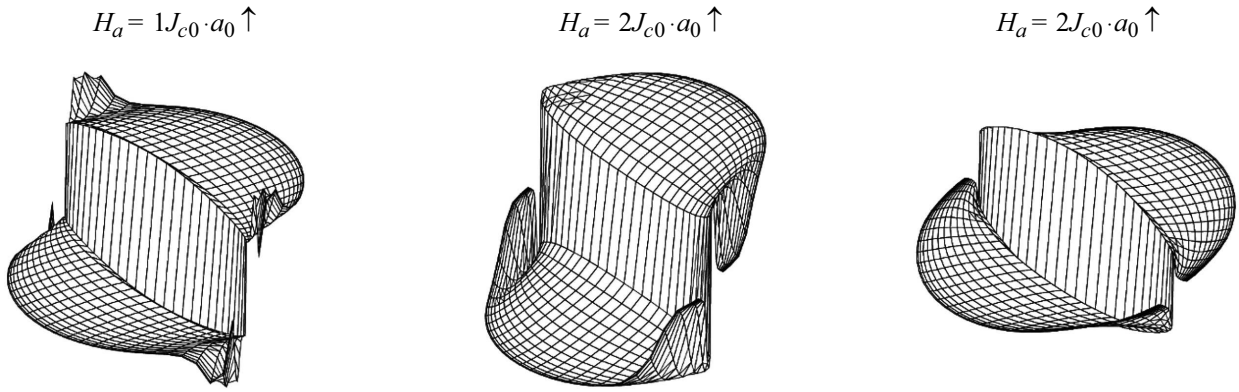

Figure 6. Current density profiles $J_c(B(r, z))$ for a ball of radius a in the Kim model with peak effect (16) for three external field values $H_a = 1J_{c0}a_0$, $2J_{c0}a_0$ and $3J_{c0}a_0$. The position of the maximum is $B_p = 2\mu_0 J_{c0}a_0$.

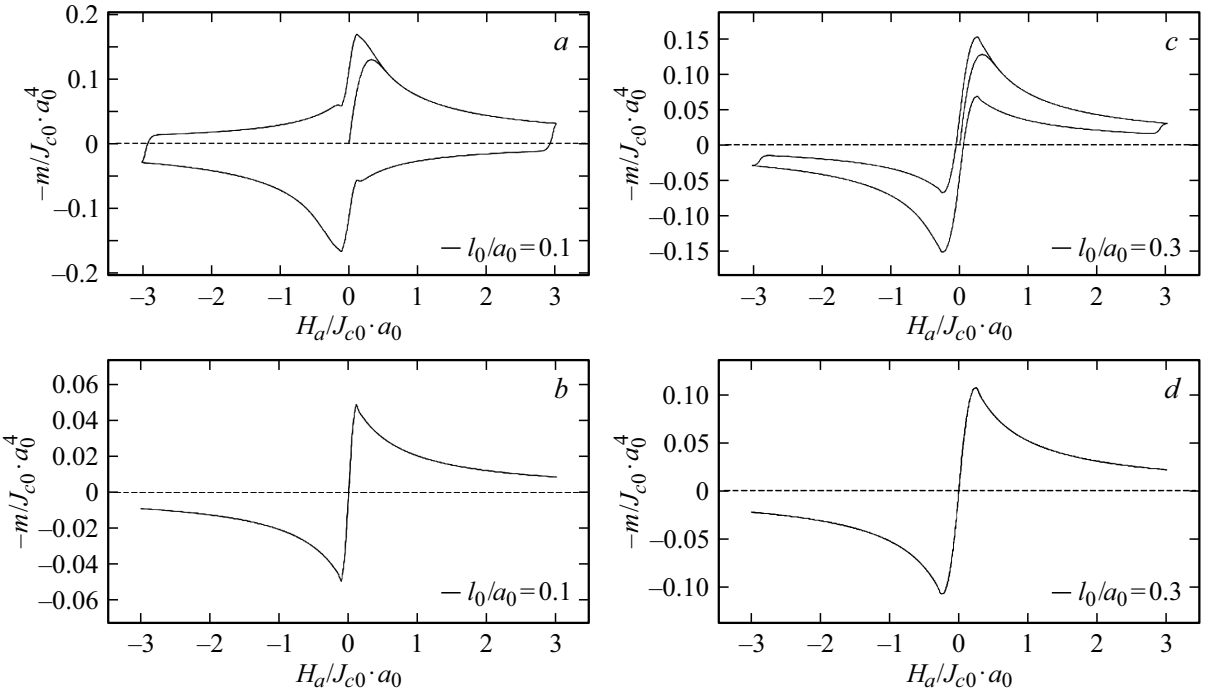

Figure 7. Magnetic moment loops of a spherical sample considering equilibrium areas of different thicknesses (a, c). The thicknesses of the equilibrium areas in the figure are given in relative units and indicated by ($l_0/a_0 = 0.1$ (a) and $l_0/a_0 = 0.3$ (c)). b, d — the magnetic moments of these equilibrium areas are given. Kim's model was used (10) with parameters $B_0 = 0.5\mu_0 J_{c0}a_0$.

ductor state, and hysteresis will appear. When studying the magnetization of, for example, low-temperature [11] and polycrystalline high-temperature superconductors [19], it was found that their hysteresis loops of magnetization or magnetic moment have a marked asymmetry relative to the abscissa axis (magnetic field strength axis). The amount of asymmetry depends on the temperature. To describe the asymmetry, the authors [11] proposed to consider the equilibrium magnetization of the superconducting sample surface layer of thickness $l_0 \sim \lambda$ — the London penetration depth. The magnetization of such a layer does not depend on the prehistory of its state and will be reversible. The reasons leading to the asymmetry of the magnetization hysteresis loop are discussed in works [20–22]. These include, for example, the Meissner effect, the surface barrier, etc. This area is called the area of equilibrium magnetization in contrast to the area of the inner part filled with vortices, where magnetization will be non-equilibrium.

When calculating the magnetic properties of superconducting bodies whose dimensions are much larger than l_0 and in large fields (comparable to the field H_p), the equilibrium area can be neglected, since its contribution to the total magnetization is negligibly small. However, if we consider granular superconductors, the value l_0 may be of an order comparable to the size of the granules. This

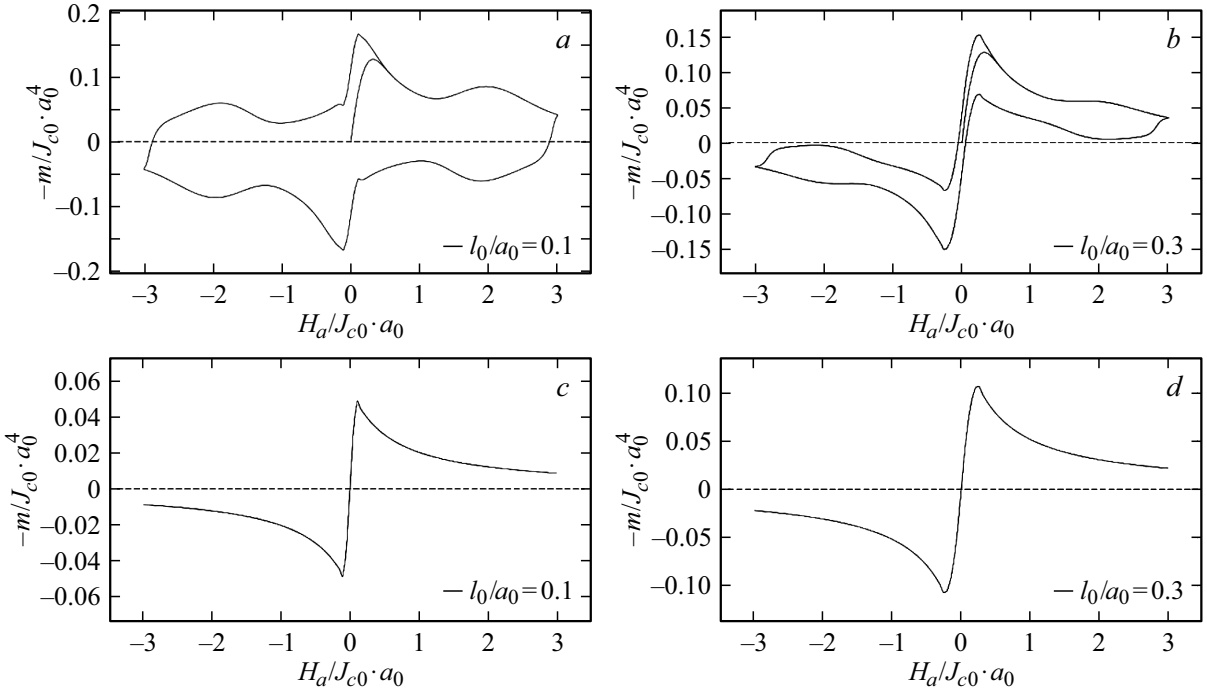

Figure 8. Magnetic moment loops of the whole sample (a, b), surface layer (c, d). The data are given for the width of the equilibrium magnetization zone equal to $l_0/a_0 = 0.1$ (a, c), 0. 3 (b, d), peak function (16), Kim model (10), using parameters $B_0 = 0.5\mu_0 J_{c0} a_0$, $A = 0.3$, $B_p = 2\mu_0 J_{c0} a_0$, $B_w = 0.5\mu_0 J_{c0} a_0$.

leads to a noticeable asymmetry of the magnetization loops, and the greater the ratio of the depth of the near-surface area to the size of the sample granules, the stronger it is expressed [12].

In the present work, we present the calculation of magnetization loops, taking into account the equilibrium area on the basis of the methodology mentioned above. In contrast to the works [13–16,20–22], in which the calculation method is valid for samples with zero demagnetizing factor, the calculation of hysteresis loops of magnetic moment was performed according to the previously obtained distribution of the critical current density in the sample on the basis of equation (6). In this case, the demagnetizing field is taken into account without additional restrictions.

The calculation was carried out so that the current distribution in the equilibrium area depended only on the direction and value of the external magnetic field, but not on the sign of its rate of change. For this purpose, at the first stage, when the field increases from zero to its maximum value by the program, the values of local current densities in the cells included in the near-surface layer are recorded. With further modifications, these data are used to calculate the full magnetic response of the sample. Figure 7 shows the results of calculating the magnetic moment loops of a spherical sample of radius a_0, as well as the profiles of the local magnetic field induction for the central section. Note, that the asymmetry of the magnetic moment loop with respect to the horizontal level ($m = 0$, abscissa axis) increases with increasing values of the near-surface layer depth.

As indicated in [22], the problem with equilibrium magnetization becomes more complicated in the presence of a peak effect in the sample. Since the vortices do not experience in the near-surface area the same fixation as in the inner area, the secondary magnetization peak should not appear there and increase the asymmetry of the loop. To compensate for this phenomenon, the author of the aforementioned paper proposes to change the depth of the equilibrium area, reducing it at the secondary peak. In the present work, a different approach was used: when calculating the sample magnetization with allowance for the peak effect and the equilibrium area, the currents in the near-surface zone were first determined without considering the peak effect, and then, the obtained data were used for full simulation.

The calculation results for the near-surface zone are shown in Fig. 8. As can be seen, the peak effect does not affect the equilibrium magnetization area.

Conclusion

Thus, in this work, we have performed numerical simulations of the magnetic properties of axisymmetric pellet superconductors of the second kind for a number of models of dependence of the critical current density on the magnetic field induction (10)–(12), taking into account the pick effect and equilibrium magnetization. Different

variants of the functions (14)–(16) were used as peak functions. The magnetic moment loops of the samples were determined directly by integrating over time the integral equation for current density obtained using the critical state concept based on the equations of electrodynamics. Calculation of the magnetic field at each point for each iteration step allowed us to use different dependences of the critical current on the local magnetic field induction and peak functions. The current density profiles $J_c(B)$ in the Kim model with the logistic peak-function (16) and the equilibrium magnetic moment of spherical pellets were also calculated. The method of calculating the magnetic moment used in this work allows the equilibrium and nonequilibrium areas of the sample to be taken into account independently.

The results of calculating the hysteresis loops $m(H_a)$ and $B(H_a)$ show that the dependence $J_c(B)$ (11) leads, as might be expected, to wider loops due to the slower decline of the function $J_c(B)$. It is obtained that ellipsoidal samples stretched along the symmetry axis require a smaller penetration field H_p, while flattened ones require a larger one. It should also be noted that all three peak functions (14)–(16) have no significant effect on the magnetic moment hysteresis loops. The results of the calculation of the magnetic moment loops of a spherical sample of radius a_0, as well as the local magnetic field induction profiles for the central section showed that the asymmetry of the magnetic moment loop relative to the horizontal level ($m = 0$, abscissa axis) increases with increasing values of the near-surface layer width.

Conflict of interest

The authors declare that they have no conflict of interest.

References

[1] P. Bean. Phys. Rev. Lett., **8**, 250 (1962). DOI: 10.1103/PhysRevLett.8.250
[2] E.H. Brandt. Phys. Rev. B, **54**, 4246 (1996). DOI: 10.1103/PhysRevB.54.4246
[3] E.H. Brandt. Phys. Rev. B, **58**, 6506 (1998). DOI: 10.1103/PhysRevB.58.6506
[4] N.D. Kuz'michev, A.A. Fedchenko. Tech. Phys., **57** (5), 631 (2012). DOI: 10.1134/S1063784212050180
[5] N.D. Kuzmichev, A.A. Shushpanov, M.A. Vasyutin. Journal of SVMO, **22** (4), 456 (2020). DOI: 10.15507/2079-6900.22.202004.456-462
[6] G.F. Zharkov. Phys. Usp., **47**, 944 (2004). DOI: http://dx.doi.org/10.1070/PU2004v047n09ABEH001875
[7] G.F. Zharkov, V.G. Zharkov, A.Yu. Zvetkov. Phys. Rev. B, **61**, 12293 (2000). DOI: 10.1103/PhysRevB.61.12293
[8] A. Gulian. *Shortcut to Superconductivity. Superconducting Electronics via COMSOL Modeling* (Springer, 2020), DOI: 10.1007/978-3-030-23486-7
[9] V.Ya. Arsenin. *Methods of mathematical physics and special functions* (Nauka, M., 1984)
[10] Y.B. Kim, C.F. Hempstead, A. Strand. Phys. Rev. Lett., **129**, 528 (1963). DOI: 10.1103/PhysRev.129.528
[11] W.A. Fietz, M.R. Beasley, J. Silcox, W.W. Webb. Phys. Rev., **136**, A335 (1964). DOI: 10.1103/PhysRev.136.A335
[12] F. Irie, K. Yamafuji. J. Phys. Soc. Jpn., **23**, 255 (1967). DOI: 10.1143/JPSJ.23.255
[13] E.W. Urban. J. Appl. Phys., **42**, 115 (1971). DOI: 10.1063/1.1659540
[14] V.V. Valkov, B.P. Khrustalev. ZhETF, **107** (4), 1221 (1995).
[15] D.A. Balaev, D.M. Gokhfeld, S.I. Popkov, K.A. Shaykhutdinov, L.A. Klinkova, L.N. Zherikhina, A.M. Tvokhrebov. ZhETF, **145** (1), 120 (2014). DOI: 10.7868/S004445101401012X
[16] T.H. Johansen, M.R. Koblischka, H. Blatsberg, P.O. Hetland. Phys. Rev. B, **56**, 11273 (1997). DOI: 10.1103/PhysRevB.56.11273
[17] D.G. Kulkarni, K.V. Bhagwat, G. Ravikumar. Physica C., **391**, 178 (2003). DOI: http://dx.doi.org/10.1016/S0921-4534
[18] M. Jirsa, L. Pust, D. Dlouhý, M.R. Koblischka. Phys. Rev. B, **55**, 3276 (1997). DOI: 10.1103/PhysRevB.55.3276
[19] S. Senoussi, C. Aguillon, P. Manuel. Physica C, **175** (1–2), 202 (1991). DOI: 10.1016/0921-4534(93)90135-D
[20] D.-X. Chen, R.W. Cross, A. Sanchez. Cryogenics, **33**, 695 (1993). DOI: 10.1016/0011-2275(93)90022-G
[21] D.-X. Chen, R.B. Goldfarb, R.W. Cross, A. Sanchez. Phys. Rev., **48**, 6426 (1993). DOI: 10.1103/PhysRevB.48.6426
[22] D.M. Gohfeld. FTT, **56** (12), 2298 (2014). DOI: 10.1134/S1063783414120129